2023 IEEE International Conference on Robotics and Automation (ICRA 2023)
May 29 - June 2, 2023. London, UK

Real-Time Estimation of Walking Speed and Stride Length Using an IMU Embedded in a Robotic Hip Exoskeleton

Keehong Seo

Abstract— **Gait parameters, including walking speed and stride length, are crucial indicators of health status and rehabilitation progress for individuals using wearable robots for exercise or rehabilitation. These metrics play a crucial role in monitoring progress and adjusting training programs, thereby fostering greater engagement in the training. In this paper, we present methods for estimating walking speed and stride length using sensors in wearable hip exoskeleton GEMS-H.**

Our study collected data from 79 middle-aged healthy individuals walking on a treadmill while wearing GEMS-H under various assistance conditions. To estimate walking speed, we evaluated linear regression models, deep neural networks, and ensemble models using different combinations of joint encoders and an IMU in the GEMS-H hip exoskeleton to form various sets of features. The ensemble of deep neural networks using only 6-DOF IMU signals as features achieved the lowest root-mean-square error (RMSE) for walking speed estimation, which was 0.066 m/s.

We also present an algorithm for real-time stride length estimation, building on one of the speed estimation models. The speed and stride length estimation model was tested on 12 middle-aged healthy subjects walking in GEMS-H overground, yielding an RMSE of 0.060 m/s for speed and 7.1 cm for stride length.

I. INTRODUCTION

Lower-limb wearable robots have been proposed as assistive devices for individuals with ambulatory impairments [1], [2], [3], [4], [5] and as personal trainers for older adults [6], [7], [8], [9]. To facilitate their wider use, it is crucial that these devices have the capability to evaluate and monitor the physical performance of users, enabling personalized training and rehabilitation programs. This will not only motivate participant effort, but also lead to improved outcomes.

Gait speed and stride length are commonly regarded as key indicators of fitness in older adults [10], [11] and important outcome measures for rehabilitation of ambulatory patients, along with symmetry and variability [3], [12], [13]. A range of estimation methods for gait parameters have been proposed, including those based on foot-mounted IMUs[14], [15], shank-mounted IMUs [16], deep convolutional neural networks (CNNs) [17], [18], and long short-term memory (LSTM) models and autoencoders [19].

Our study focuses on estimating gait speed and stride length on a hip exoskeleton in real time by using the hip exoskeleton GEMS-H, which has been shown to be effective in supporting the ambulation of the elderly [20] and rehabilitation of stroke patients [21]. However, there are challenges in estimating gait parameters with wearable robots such as hip exoskeletons, due to limited sensor information and the presence of artifacts in the sensor data originating from exoskeleton actuation. As a result, none of the aforementioned studies can be directly implemented for GEMS-H (see Fig. 1), having only one IMU in the back unit and two joint encoders in the hip joints, all of which are affected not only by human motion but also by actuation of the motors.

We collected GEMS-H data from 79 healthy adults walking on a treadmill while wearing the exoskeleton. Deep neural networks such as CNN and LSTM were then trained using the collected data while linear regression models were trained as a baseline of the study. After investigating the 10-fold cross validation performance of individual models as well as ensembles of them, the best result was achieved with an ensemble of LSTM and CNN models with the root-mean-square error of 0.066 m/s. The trained LSTM model was then deployed in GEMS-H and a stride estimation algorithm was implemented. The overall spatiotemporal parameter estimation, running on GEMS-H in real-time, was evaluated for overground walking of 12 healthy adults, resulting in a root-mean-square error of less than 5 % for both gait speed and stride length.

The author is with Samsung Research, Samsung Electronics, 56 Sungchon-gil, Seocho-gu, Seoul, Republic of Korea
keehong.seo@samsung.com

II. SPEED ESTIMATION

To estimate gait speed with the sensors in GEMS-H, we studied three different types of models — linear regression (LR), long short-term memory (LSTM), and convolutional neural network (CNN) — and ensembles of them as we elaborated below.

A. The Device and the Control Method

Our group had developed the hip exoskeleton GEMS-H to assist the elderly and stroke patients. Since it was first introduced in the literature in [22], it has gone through modifications in design and algorithms. The version used for this study, which was not commercially available, weighed about 2.1 kg with two electrical motors placed on the hip joints that could produce instantaneous joint torques up to 8 Nm. The main board was located in the back unit, which had 1-GHz ARM Cortex-A8 as the CPU. There were two joint angle sensors to sense the motion of the hip joints and one IMU sensor on the back compartment. The location and reference direction of the IMU is shown in Fig. 1.

Its assistance algorithm was adopted from our previous work in [22] and [23]. The algorithm used an LSTM model to estimate continuous gait phase and computed sinusoidal torque output based on the gait phase. The amplitude of

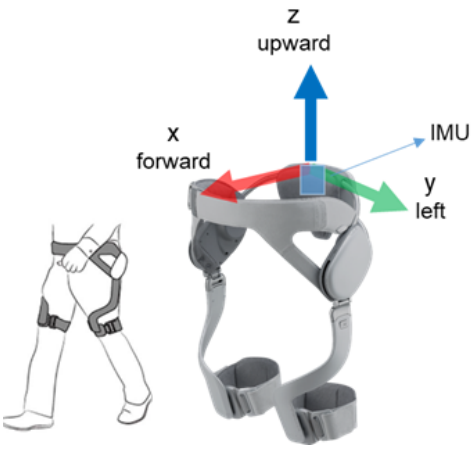

Fig. 1: The location of the IMU sensor in GEMS-H and reference directions

assistive torque was determined from the experimental protocol. The algorithm continuously adjusted the phase of torque pattern so that the negative peak of assistive torque to lag 4 % gait cycle relatively to the negative peak of joint velocity profile. The negative direction in the joint space of GEMS-H refers to the direction of hip flexion. The lag of 4 % was adopted from our study on the timing of assistive torque [24]. While running the algorithm, GEMS-H also recorded the joint angles, the joint angular velocities, 3-axis acceleration and 3-axis gyroscope values from the IMU, every 10 ms. The joint velocity was obtained from the inter-sample difference of each joint encoder data to be filtered with first order low-pass-filter with cutoff frequency at 40 Hz. IMU signals were recorded without any post-processing.

B. Data Collection

During this study, we collected GEMS-H data from 79 healthy middle-aged adults while they walked on a treadmill under various speed and assistance conditions. Only two of the participants were female. Midway through the data collection process, the protocol was modified due to a management decision that extended the maximum walking speed to 8.0 km/h.

TABLE I: The Protocol for Gait Speed Data Collection

Phase	Assistance	Speed	Duration
1		Medium	30 Strides
2	Medium	Low	30 Strides
3		High	30 Strides
4	— Stand Still —		15 seconds
5		Medium	30 Strides
6	None	Low	30 Strides
7		High	30 Strides
8		Medium	30 Strides
9	High	Low	30 Strides
10		High	30 Strides

For the first 50 subjects, we collected GEMS-H data following the protocol described in Table I. With this protocol, subjects walked at nine different conditions: 3 speeds $\times$ 3 assistance levels through phase 1 to 10 in the table. For each subject, the assistance level was randomly selected from 6 to 10 for 'medium', and from 11 to 15 for 'high'. 'None' refers to zero-torque output. The assistance level 15 translated to 6 Nm for the peak of the sine wave of the assistive torque. The treadmill speed was randomly selected from 1.0 to 2.4 km/h for 'low', from 2.5 to 3.9 km/h for 'medium', and from 4.0 to 5.3 km/h for 'high'. At phase four in Table I, subjects stood still on the treadmill for 15 seconds, which was labeled as 0 m/s. Other phases lasted for 30 strides. GEMS-H software changed the assistance level by counting the strides, and it prompted the target treadmill speed on a display so that our staff could adjust the treadmill speed accordingly.

For the other 29 subjects, we increased the maximum speed and changed the protocol. In this protocol, once a subject started walking on the treadmill at 5.5 km/h, the staff gradually increased the treadmill speed to the individual maximum, without exceeding 8.0 km/h, and then decreased back to 5.5 km/h. The process was done once with assistive torque and then with zero-torque. The treadmill speed, which was adjusted as much as 0.3 or 0.4 km/h every 10 strides, was recorded manually through a mobile app, connected to GEMS-H software.

Overall, the dataset collected from 79 subjects contained more than 28,000 strides.

C. Linear Regression and Feature Selection

First, we evaluated LR models to establish a baseline of the speed estimation, and to gain insights on the correlation of the input features. To compute the features over each stride, we identified the beginnings of strides by detecting the zero–crossings of the left joint angular velocities that had been moving averaged over a 0.5-second window. We then constructed six groups of features from the linear accelerations and angular velocities in the x/y/z-axis of the IMU, and the joint angles and joint angular velocities of the left and right joints as listed in Table II.

TABLE II: The Groups of Candidate Features

Group	Description	Dimension
1	the SDs[a] of accelerations from the IMU	3
2	the SDs of angular velocities from the IMU	3
3	the mean of the SDs of the left and right joint velocities	1
4	the mean of the minima (and maxima) of the left and right joint velocities	2
5	the mean of the SDs of the joint angles of the left and right joints	1
6	the mean of the minima (and maxima) of the left and right joints	2

[a]SD stands for standard deviation.

LR models with first, second, and third order polynomials for all the possible combinations of the six feature groups were evaluated. For this, we partitioned the dataset into 10

groups for 10-fold cross validation[1], where we ensured data from any subject would be found only at one group.

The result showed that the best LR model was the one with second degree polynomials and the features from group 1, 3, 4, and 5 in Table II, whose coefficient of determination R^2 was 0.9411 with root-mean-square error (RMSE) of 0.1136 m/s. The distribution of the estimated speed with respect to the reference speed is shown in Fig. 3 in comparison with the best result of our deep neural networks introduced below.

D. Deep Neural Networks and the Ensembles

When investigating the feasibility of deep neural networks for speed estimation, we limited it to CNN, LSTM and ensembles of them. The hyperparameters were also determined after a limited number of iterations.

1) Feature Sets: As for the features, the inputs to the models, we considered two sets of features A and B based on the results from LR above. Set A consisted of the six IMU signals – three from the accelerometer and three from the gyroscope in three axes – while set B had, in addition to the six features of A, the four signals of the left and right joint angles and angular velocities. The names of models in our study had either A or B in them to identify the feature sets used in training. All the feature signals were normalized for training by their means and standard deviations of the whole dataset.

2) CNN Models: Similar to the CNN model in [18], we configured ours to have four 1-dimensional convolution layers and two fully connected (FC) layers. The convolution layers all had the kernel of size 10 with stride of one. Each was followed by a 1-dimensional batch normalization and a ReLU, and the fourth convolution layer had an average pooling layer of size four. The number of channels doubled through each of the first two convolution layers while it decreased by half through each of the last two. Input signals were limited to 100 samples on the time axis, corresponding to one second. For feature set A, the numbers of inputs to the first and second FC were 96 and 48; for feature set B, they were 120 and 60, respectively.

3) LSTM Models: Our LSTM models had a single LSTM layer with 48 hidden states and a single FC layer to yield the output of size one. The temporal length of training sequences were fixed to 960, corresponding to 9.6 seconds. It did not imply that the models, when deployed, had to wait for 960 sampling times to fill up the input sequence. In fact, the models produced one estimate speed every time a new input sequence of length one was given.

4) Domain Randomization and Hyperparameters: To prepare the models for the cases in which users wear the device tilted in arbitrary direction, we applied 3-dimensional rotational transformation to the acceleration and angular velocity from the IMU data, when training the model. The angle of rotation was randomly selected between -11.5 and +11.5 degrees.

[1]In the 10-fold cross validation, once a model is trained with data from nine groups, it is then tested with the 10th group that wasn't used for from training, and this process repeats 10 times until all the 10 groups take turns to be the test group.

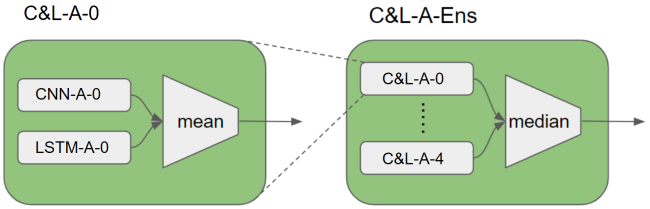

(a) A C&L ensemble was constructed by averaging a CNN model and an LSTM model. A homogeneous ensemble of such C&L models are also shown.

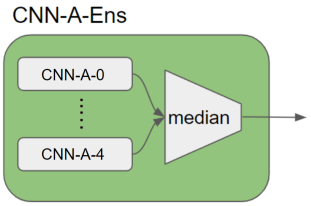

(b) A homogeneous ensemble CNN-A-Ens was built from the median output of five models of the same type.

Fig. 2: Construction of Ensemble Models

For both LSTM and CNN models, we used MSE loss and Adam optimizer, and the training data was randomly loaded allowing replacement. The number of epochs was 80 for CNNs, and 100 for LSTMs. Learning rate started at 0.001, and it decreased by the factor of 0.2 (0.5) after 50 (40) epochs for CNNs (LSTMs). Batch size was 32 for CNNs and 24 for LSTMs.

5) The Ensembles of the Models: We experimented with two different ensembling methods. In the first method, we computed stride-wise means for both a CNN model and an LSTM model by averaging the outputs over each stride. We then computed the pairwise mean of the stride-wise means from the CNN and LSTM models, which was called 'C&L' (as shown in Fig. 2a). In the second method, we trained a group of homogeneous models, all of which were either CNNs or LSTMs, trained independently. We denoted these homogeneous ensembles with 'Ens' in their names and computed them as the medians of stride-wise means of the models in the group as shown in Fig. 2b.

6) Evaluation: We trained and validated the CNN and LSTM models for both feature sets A and B five times, resulting in the models CNN(LSTM)-A(B)-0 to CNN(LSTM)-A(B)-4. To evaluate the models, we used 10-fold cross validation, as described in the previous section on linear regression, and measured performance using metrics such as R^2 and RMSE on the stride-wise averaged outputs. We also evaluated the performances of pairwise ensemble models C&L-A(B)-0 to C&L-A(B)-4 as well as homogeneous ensemble models such as CNN-A(B)-Ens, LSTM-A(B)-Ens and C&L-A(B)-Ens.

E. The Results and Analysis

Table III shows the R^2 and RMSE values for the LR, CNN, LSTM, and ensemble models. For non-ensemble models and

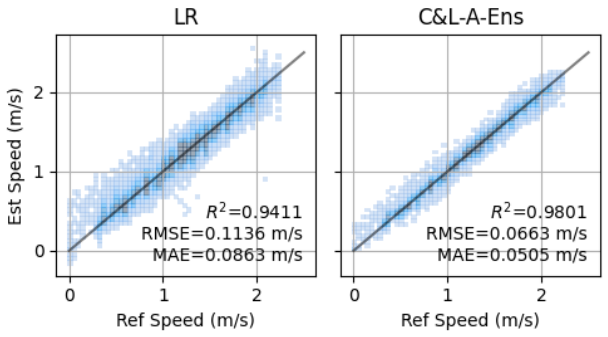

Fig. 3: Results of 10-fold cross validation, averaged for each stride, are shown for LR and C&L-A-Ens.

C&L models, we aggregated the stride-wise outputs from the five evaluations to compute their performance metrics. The model that performed best was a pairwise ensemble C&L-A-Ens, with an R^2 of 0.98 and an RMSE of 0.066 m/s, whose output distribution is compared with the LR model above in Fig. 3. The best performing non-ensemble models were LSTM-A and CNN-B, which showed very close performance although LSTM-A showed larger variation as shown in Fig. 4. From the evaluation results, we made following observations.

1) Linear Regression vs. Deep Neural Networks: From the result above, the deep models CNNs and LSTMs showed superior performance to LRs. The R^2 values were greater than 0.975 for all the LSTM and CNN models while it was 0.940 for LR.

2) The Feature Sets A vs. B: Regarding the input features to the CNNs and LSTMs, we compared the RMSEs of two groups of non-ensemble models: one using set A for input, and the other using set B. The result of independent t-test indicated that one was not significantly better than the other ($p = 0.37$)

3) LSTM vs. CNN: Comparison between the non-ensemble LSTMs and CNNs did not show significant difference from an independent t-test ($p = 0.38$). When we applied independent t-tests for all the possible pairs of models from CNN-A, CNN-B, LSTM-A, and LSTM-B, the only pair that showed p-value less than 0.05 was CNN-A versus CNN-B ($p = 0.024$). For CNN models, we could see that using the joint encoders and the IMU together had advantage over using the IMU only. The distributions of the metrics with respect to the model types and feature sets are shown in Fig. 4.

4) The C&L Pairwise Ensembles : All the C&L pairwise ensembles, C&L-A(B)-0(1,2,3,4) showed significantly lower RMSE (and higher R^2) values than the individual CNN or LSTM models did, as shown in Fig. 5. The paired t-test between either the group of CNN or LSTM models against the group of the C&L models resulted in $p = 0.00$.

5) The Homogeneous Ensembles: When we compared the metrics of the homogeneous ensembles CNN(LSTM,C&L)-A(B)-Ens with the metrics of individual models

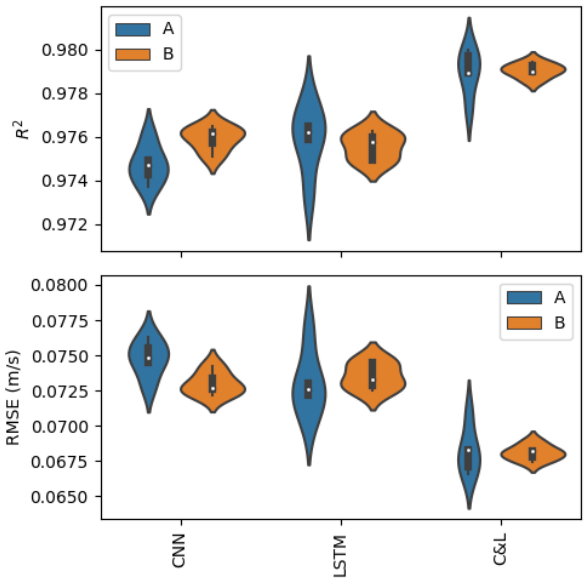

Fig. 4: The violin plot shows the different performance of models – CNN, LSTM, and C&L – with feature sets A and B. Each violin, around a conventional box plot, presents the distribution of the metrics from training each model for five times.

CNN(LSTM,C&L)-A(B)-0(1,2,3,4), the 'Ens' versions always outperformed the individual models as we illustrated in Fig. 5.

From the evaluation of individual and ensembled models, we observed that the C&L pairwise ensembles performed better than single CNN or LSTM models; and that the homogeneous ensembles C&L-A-Ens or C&L-B-Ens was better than single C&L-A or C&L-B models, making C&L-A-Ens and C&L-B-Ens the best models.

III. STRIDE LENGTH ESTIMATION

Once the gait speed is estimated as explained above, stride length can be computed from

$$(Stride\ Length) = (Stride\ Speed) \times (Stride\ Time), \quad (1)$$

where 'stride speed' is the average of walking speed over a stride and 'stride time' is the period of the stride. Among various methods to detect stride period in real time such as [22], [25], [26], [27], [28], [29], we used LSTM-based gait phase estimation, introduced with the ankle exoskeleton GEMS-A in [23], after some modification to use joint encoders instead of an IMU. For speed estimation, we trained an LSTM-A model[2] with the whole dataset from 79 subjects introduced above. In this section, we introduce an overground experiment that evaluated both the speed and stride length estimation of ours by using a sensorized mat as ground truth.

[2]We selected LSTM-A for this experiment because, at the time, we had not yet studied LSTM-B, CNN-A(B), or their ensembles.

TABLE III: Evaluation of the models.

	CNN-A	CNN-B	LSTM-A	LSTM-B	C&L-A	C&L-B	LR
R^2	0.9747	0.9759	0.9759	0.9756	0.9790	0.9791	0.9411
RMSE (m/s)	0.0748	0.0730	0.0730	0.0735	0.0682	0.0681	0.1136
	CNN-A-Ens	CNN-B-Ens	LSTM-A-Ens	LSTM-B-Ens	C&L-A-Ens	C&L-B-Ens	
R^2	0.9765	0.9773	0.9784	0.9775	**0.9801**	0.9799	
RMSE (m/s)	0.0722	0.0709	0.0691	0.0706	**0.0663**	0.0667	

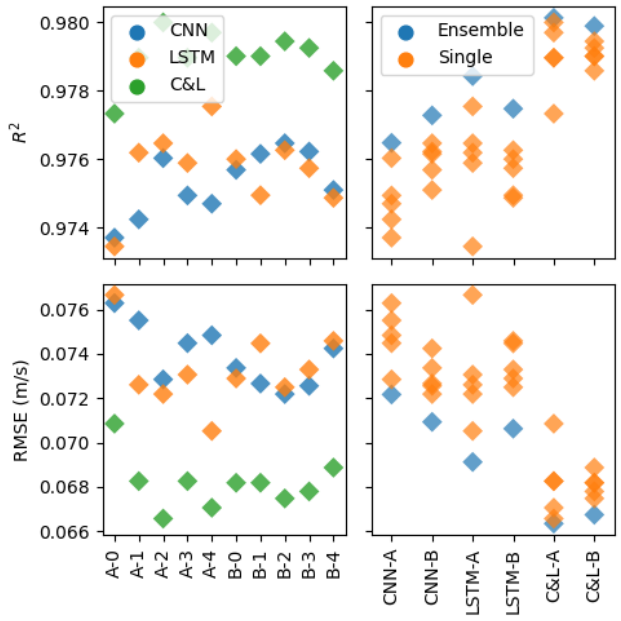

Fig. 5: The left side of the plot shows the R^2 and RMSE of individual CNN and LSTM models, as well as their C&L pairwise ensembles. We observed that the error significantly decreased ($p = 0.00$ when paired t-test) when ensembling a pair of CNN and LSTM. On the right side of the plot, individual models and their homogeneous ensembles are displayed. We found that training the same model five times and ensembling them resulted in lower error compared to any of the individual models. This observation also applies to C&Ls, which can be considered as an ensemble of ensembles.

A. The Overground Walking Experiment

Twelve male subjects, middle-aged without major health issues, participated in the experiment. Participants wore GEMS-H and walked on an 8-meter GAITRite sensor mat (CIR Systems, Inc., United States) to record spatiotemporal gait parameters, including stride speed, stride length, and stride time, as shown in Fig. 6.

For this experiment, participants walked on the mat at three self-selected speeds - 'slow', 'medium', and 'fast' - under three different assistance modes: 'zero-torque', 'assistance', and 'resistance'. Participants began walking approximately three strides prior to entering the mat and continued for approximately two strides after walking out of the mat. Regarding the assistance algorithm, we used one in [30]

Fig. 6: A subject is walking on a GAITRite system wearing GEMS-H, the hip exoskeleton.

for this experiment. During the walking sessions, GEMS-H estimated walking speed, stride time, and stride length in real time at a sampling rate of 100 Hz, and recorded the data. In total, there were 109 walking sessions across all participants, consisting of 662 strides.

B. The Results and Discussion

The estimated speed, stride, and stride length, as recorded by GEMS-H, were compared with the measurement from GAITRite, shown in Fig. 7. The values of R^2, RMSE, and mean absolute error (MAE) are listed in Table. IV.

TABLE IV: Stride Length Estimation on Overground Surface

	RMSE	%-RMSE	MAE	%-MAE
Speed	0.0603 m/s	4.4482 %	0.0458 m/s	3.4370 %
Stride Time	0.0232 s	2.1155 %	0.0169 s	1.5168 %
Stride Length	7.0589 cm	4.8437 %	5.4943 cm	3.7686 %

We noticed that the RMSE in our overground speed estimation was 0.060 m/s while, from the 10-fold cross validation in III, the same method of LSTM-A showed an RMSE of 0.073 m/s and the best method of C&L-A-Ens showed an RMSE of 0.066 m/s. When compared to the results in the literature, an RMSE of 0.060 m/s was comparable to an RMSE of 0.080 m/s in [16], where a shank-mounted IMU and double integrals were used. Our overground dataset was smaller in size and had a more limited range of speeds compared to our treadmill dataset. Despite this, our overground experiment showed that the speed estimation model could potentially extend to overground gait speed estimation.

The stride time estimation also showed reasonable performance with RMSE of 2.12 %, which was better than speed

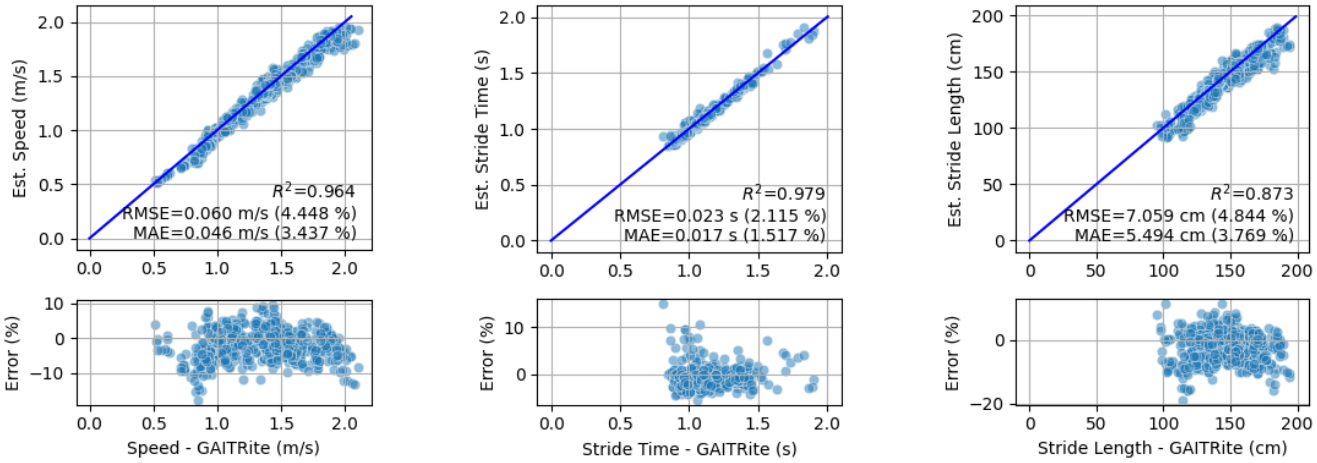

(a) Walking Speed Estimation

(b) Stride Time Estimation

(c) Stride Length Estimation

Fig. 7: Estimated spatiotemporal gait parameters from overground walking are plotted. Errors are plotted in % for comparison between different units.

estimation RMSE of 4.45 %. The stride length estimation resulted in an RMSE of 4.84 % slightly greater than speed estimation, which made sense because uncertainties in speed estimation and stride time estimation interact with each other multiplicatively.

When compared with results from previous studies, our stride length estimation with an RMSE of 4.84 % (7.06 cm) and an MAE of 3.77 % (5.49 cm) was comparable to an MAE of 4.63 % in [19]; or to an MAE of 2.89 cm in [18] where *step* length was estimated using multiple IMUs. Despite differences in experimental settings between our study and these previous works, the comparison of RMSE and MAE values demonstrates that our method for estimating stride length achieves acceptable accuracy and is competitive with state-of-the-art approaches in the field.

IV. CONCLUSION

The accurate prediction of gait speed and stride length is essential for evaluating gait abnormalities and monitoring progress during rehabilitation programs. In recent years, the use of wearable sensors and exoskeletons has become an increasingly popular approach for measuring gait parameters. This study has contributed to this field by demonstrating the potential of deep neural network models to estimate gait parameters in real time using sensor data from a hip exoskeleton, regardless of the level of assistance power. The contributions of this work can be summarized as follows:

1) The development of a deep neural network model that can estimate gait parameters with reasonable accuracy in real-time using data from a hip exoskeleton.
2) The demonstration that the model can accurately estimate gait speed and stride length using only an IMU sensor embedded in the hip exoskeleton.
3) The identification of an ensemble of models as the best approach for speed estimation, and the comparison of the performance of LSTMs and CNNs on two different feature sets.
4) The promising accuracy of the proposed method in estimating overground gait speed and stride length, indicating its potential for personalized training and rehabilitation programs using wearable robots.

However, this study has some limitations. Firstly, all participants were healthy adults without known gait impairments, which may not have accounted sufficiently for asymmetric or irregular gaits. Secondly, the method of labeling the walking speed lacked precision. Finally, our models were trained only for flat and straight paths, and further work is required to extend it to various paths such as curved or inclined ones.

To build on the results of this study, several potential directions for future work were identified. Firstly, the proposed method could be applied on a larger and more diverse population, including individuals with gait impairments, to evaluate its generalizability and robustness. Secondly, the method could be extended to different types of exoskeletons, sensor configurations, and gait paths to improve the applicability and flexibility of the method. Finally, incorporating the proposed method into a closed-loop system for adaptive assistance and control of exoskeletons could potentially improve the efficiency and efficacy of gait rehabilitation and training.

REFERENCES

[1] F. Giovacchini *et al.*, "A light-weight active orthosis for hip movement assistance," in *Robotics and Autonomous Systems*, vol. 73, 2015, pp. 123–134.

[2] H. Tanaka *et al.*, "Spatiotemporal gait characteristic changes with gait training using the hybrid assistive limb for chronic stroke patients," *Gait & Posture*, vol. 71, pp. 205–210, 2019.

[3] K. Tomida *et al.*, "Randomized Controlled Trial of Gait Training Using Gait Exercise Assist Robot (GEAR) in Stroke Patients with Hemiplegia," *Journal of Stroke and Cerebrovascular Diseases*, vol. 28, no. 9, pp. 2421–2428, 2019.

[4] D. R. Louie, J. J. Eng, and T. Lam, "Gait speed using powered robotic exoskeletons after spinal cord injury: a systematic review and correlational study," *Journal of NeuroEngineering and Rehabilitation*, vol. 12, no. 1, p. 82, 2015.

[5] D. R. Louie and J. J. Eng, "Powered robotic exoskeletons in post-stroke rehabilitation of gait: a scoping review," *Journal of NeuroEngineering and Rehabilitation*, vol. 13, no. 1, p. 53, 2016.

[6] H. Shimada *et al.*, "Effects of a robotic walking exercise on walking performance in community-dwelling elderly adults." *Geriatrics & gerontology international*, vol. 9, no. 4, pp. 372–81, 2009.

[7] E. Martini *et al.*, "Gait training using a robotic hip exoskeleton improves metabolic gait efficiency in the elderly," *Scientific Reports*, vol. 9, no. 1, p. 7157, 2019.

[8] S. Jin, X. Xiong, D. Zhao, C. Jin, and M. Yamamoto, "Long-Term Effects of a Soft Robotic Suit on Gait Characteristics in Healthy Elderly Persons," *Applied Sciences*, vol. 9, no. 9, p. 1957, 2019.

[9] X. Hu *et al.*, "A Soft Robotic Intervention for Gait Enhancement in Older Adults," *IEEE Transactions on Neural Systems and Rehabilitation Engineering*, vol. 29, pp. 1838–1847, 2021.

[10] S. Studenski, "Gait Speed and Survival in Older Adults," *JAMA*, vol. 305, no. 1, p. 50, 2011.

[11] D. K. White *et al.*, "Trajectories of Gait Speed Predict Mortality in Well-Functioning Older Adults: The Health, Aging and Body Composition Study," *The Journals of Gerontology Series A: Biological Sciences and Medical Sciences*, vol. 68, no. 4, pp. 456–464, 2013.

[12] A. Pennycott, D. Wyss, H. Vallery, V. Klamroth-Marganska, and R. Riener, "Towards more effective robotic gait training for stroke rehabilitation: a review," *Journal of NeuroEngineering and Rehabilitation*, vol. 9, no. 1, p. 65, 2012.

[13] C. Buesing *et al.*, "Effects of a wearable exoskeleton stride management assist system (SMA®) on spatiotemporal gait characteristics in individuals after stroke: a randomized controlled trial," *Journal of NeuroEngineering and Rehabilitation*, vol. 12, no. 1, p. 69, 2015.

[14] E. Foxlin, "Pedestrian Tracking with Shoe-Mounted Inertial Sensors," *IEEE Computer Graphics and Applications*, vol. 25, no. 6, pp. 38–46, 2005.

[15] A. Mannini and A. M. Sabatini, "Walking speed estimation using foot-mounted inertial sensors: Comparing machine learning and strap-down integration methods," *Medical Engineering and Physics*, vol. 36, no. 10, pp. 1312–1321, 2014.

[16] Q. Li, M. Young, V. Naing, and J. M. Donelan, "Walking speed estimation using a shank-mounted inertial measurement unit." *Journal of Biomechanics*, vol. 43, no. 8, pp. 1640–1643, 2010.

[17] M. Sharifi Renani, C. A. Myers, R. Zandie, M. H. Mahoor, B. S. Davidson, and C. W. Clary, "Deep Learning in Gait Parameter Prediction for OA and TKA Patients Wearing IMU Sensors," *Sensors*, vol. 20, no. 19, p. 5553, 2020.

[18] H. Jin, I. Kang, G. Choi, D. D. Molinaro, and A. J. Young, "Wearable Sensor-Based Step Length Estimation During Overground Locomotion Using a Deep Convolutional Neural Network," in *2021 43rd Annual International Conference of the IEEE Engineering in Medicine & Biology Society (EMBC)*. IEEE, 2021, pp. 4897–4900.

[19] Q. Wang, L. Ye, H. Luo, A. Men, F. Zhao, and Y. Huang, "Pedestrian Stride-Length Estimation Based on LSTM and Denoising Autoencoders," *Sensors*, vol. 19, no. 4, p. 840, 2019.

[20] H.-J. Lee *et al.*, "A Wearable Hip Assist Robot Can Improve Gait Function and Cardiopulmonary Metabolic Efficiency in Elderly Adults." *IEEE transactions on neural systems and rehabilitation engineering*, vol. 25, no. 9, pp. 1549–1557, 2017.

[21] ——, "Training for Walking Efficiency With a Wearable Hip-Assist Robot in Patients With Stroke," *Stroke*, vol. 50, no. 12, pp. 3545–3552, 2019.

[22] K. Seo, S. Hyung, B. K. Choi, Y. Lee, and Y. Shim, "A new adaptive frequency oscillator for gait assistance," in *2015 IEEE International Conference on Robotics and Automation (ICRA)*. IEEE, 2015, pp. 5565–5571.

[23] K. Seo *et al.*, "RNN-Based On-Line Continuous Gait Phase Estimation from Shank-Mounted IMUs to Control Ankle Exoskeletons," in *2019 IEEE 16th International Conference on Rehabilitation Robotics (ICORR)*, vol. 2019-June. IEEE, 2019, pp. 809–815.

[24] J. Lee, K. Seo, B. Lim, J. Jang, K. Kim, and H. Choi, "Effects of assistance timing on metabolic cost, assistance power, and gait parameters for a hip-type exoskeleton," in *2017 International Conference on Rehabilitation Robotics (ICORR)*. IEEE, 2017, pp. 498–504.

[25] X. Wu, Y. Ma, X. Yong, C. Wang, Y. He, and N. Li, "Locomotion Mode Identification and Gait Phase Estimation for Exoskeletons during Continuous Multi-locomotion Tasks," *IEEE Transactions on Cognitive and Developmental Systems*, pp. 1–1, 2019.

[26] I. Kang, P. Kunapuli, and A. J. Young, "Real-Time Neural Network-Based Gait Phase Estimation Using a Robotic Hip Exoskeleton," *IEEE Transactions on Medical Robotics and Bionics*, vol. 2, no. 1, pp. 28–37, 2020.

[27] Y. Qian *et al.*, "Predictive Locomotion Mode Recognition and Accurate Gait Phase Estimation for Hip Exoskeleton on Various Terrains," *IEEE Robotics and Automation Letters*, vol. 7, no. 3, pp. 6439–6446, 2022.

[28] J. C. Perez-Ibarra, H. Williams, A. A. G. Siqueira, and H. I. Krebs, "Real-Time Identification of Impaired Gait Phases Using a Single Foot-Mounted Inertial Sensor: Review and Feasibility Study," *2018 7th IEEE International Conference on Biomedical Robotics and Biomechatronics (Biorob)*, pp. 1157–1162, 2018.

[29] T. Yan *et al.*, "A novel adaptive oscillators-based control for a powered multi-joint lower-limb orthosis," in *2015 IEEE International Conference on Rehabilitation Robotics (ICORR)*. IEEE, 2015, pp. 386–391.

[30] B. Lim, J. Jang, J. Lee, B. Choi, Y. Lee, and Y. Shim, "Delayed Output Feedback Control for Gait Assistance and Resistance Using a Robotic Exoskeleton," *IEEE Robotics and Automation Letters*, vol. 4, no. 4, pp. 3521–3528, 2019.